# Coincidence Imaging Using 2 Dual-Head γ-Camera Systems, With and Without Attenuation Correction

Einat Even-Sapir, MD, DSc[1]; Bella Yuzefovich, DSc[2]; Elka Miller, MD[3]; Jean-Paul Bouhnik, PhD[2]; Osnat Zak, MSc[2]; Hedva Lerman, MD[1]; Genady Lievshitz, MD[1]; and Charles Levin, MD[3]

[1]*Department of Nuclear Medicine, Tel-Aviv Sourasky Medical Center, Sackler Faculty of Medicine, Tel-Aviv University, Tel-Aviv, Israel;* [2]*Division of Functional Imaging, General Electric Medical System, Haifa, Israel; and* [3]*Department of Radiology, Tel-Aviv Sourasky Medical Center, Sackler Faculty of Medicine, Tel-Aviv University, Tel-Aviv, Israel*

***Objective:*** Coincidence imaging enhances the potential for imaging a greater number of patients with $^{18}$F-FDG in centers that do not have dedicated PET systems. The purpose of this study was to compare, in a clinical setting, coincidence imaging for tumor detection using 2 dual-head γ-camera systems, one equipped with a 5/8-in. (16 mm) detector (CoDe5) and the other equipped with a newly designed 1-in. (25.4 mm) detector (CoDe8) with an x-ray tube installed in its gantry.

***Methods:*** Thirty consecutive patients were studied by both systems during the same visit and had 4 image sets for comparison: CoDe5 without attenuation correction (CoDe5NC), CoDe8 with (CoDe8AC) and without (CoDe8NC) attenuation correction, and fused coincidence-CT images. The target-to-background ratio (T/Bg ratio) and target-to-nontarget ratio (T/NT ratio) were calculated for each tumor site.

***Results:*** On visual assessment, 61 tumor sites were detected on CoDe8AC images. Of these, 59 (97%) were detected on CoDe8NC and 54 (88%) were detected on CoDe5NC images. Fused images improved image interpretation in 10 patients (33%) compared with coincidence images alone. Data added by fusion were of clinical relevance in 6 patients (20%). On quantitative assessment, the number of accepted events by the CoDe8 was significantly higher than that by CoDe5 (5.21 ± 1.46 million vs. 1.27 ± 0.36 million, $P < 0.001$). When comparing CoDe5 with CoDe8 images without attenuation correction, the T/Bg and T/NT ratios were significantly higher on the CoDe8 images ($P < 0.0005$ and $P < 0.0005$, respectively). When comparing CoDe8 images with and without attenuation correction, the T/Bg ratio was better on the attenuation-corrected images ($P < 0.0005$).

***Conclusion:*** Coincidence imaging with 1-in. detectors and attenuation correction improve image quality and, to a lesser extent, the tumor detection rate compared with the 5/8-in. detectors and noncorrected images. The data added by fusion of coincidence images to CT findings were clinically relevant in 20% of the patients.

***Key Words:*** coincidence imaging; $^{18}$F-FDG; γ-camera; PET; neoplasms

***J Nucl Med Technol 2004; 32:190–197***

Assessments using $^{18}$F-FDG have been shown to provide data that are of clinical importance in patients with various malignant diseases. $^{18}$F-FDG studies can now be performed not only by dedicated PET systems but also by γ-cameras modified to operate in the coincidence detection (CoDe) mode as well (*1–4*). The data added by a CoDe $^{18}$F-FDG assessment have been shown to be of clinical value in various human malignancies, including non–small cell lung cancer, recurrent colorectal carcinoma, lymphoma, and melanoma (*4–6*).

Upgrading of γ-cameras to operate in the CoDe mode has required major alterations of the systems, including improvement of electronics, increasing the NaI(Tl) crystal thickness from the standard size of 3/8 in. (9.7 mm), the addition of attenuation correction, and the use of iterative reconstruction algorithms (*1,7–11*).

In spite of these alterations, tumor detection using dedicated PET systems is superior to that of the camera-based CoDe technique, particularly in the case of lesions <1.5 cm. In addition, image quality is better with dedicated PET systems (*2,4,8,9,12–14*). Most of the alterations that have been introduced in the new-generation γ-cameras are designed to overcome these limitations.

In the Department of Nuclear Medicine, Tel-Aviv Sourasky Medical Center, 2 dual-head γ-cameras have been

For correspondence or reprints contact: Einat Even-Sapir, MD, DSc, Department of Nuclear Medicine, Tel-Aviv Sourasky Medical Center, 6 Weizman St., Tel-Aviv, 64239 Israel.
E-mail: evensap@tasmc.health.gov.il

used for CoDe of $^{18}$F-FDG, one equipped with 5/8-in. (16 mm) NaI(Tl) detectors (CoDe5) and the other equipped with newly designed 1-in. (25.4 mm) NaI(Tl) detectors (CoDe8). In the latter system, a low-dose x-ray tube was installed in the gantry, allowing for transmission and emission acquisitions to be performed at the same setting without changing the patient's positioning. The transmission data are used for both attenuation correction and for the generation of fused functional–anatomic image sets. Iterative reconstruction is available in both systems. The purpose of this study was to compare, in a clinical setting of tumor detection, the performance of the 2 coincidence γ-cameras. Thirty consecutive patients referred for an $^{18}$F-FDG study were imaged by both cameras during the same visit, allowing a direct comparison of the scintigraphic findings.

## MATERIALS AND METHODS

### Patients

Thirty consecutive patients referred for a coincidence $^{18}$F-FDG study were enrolled, including 29 patients with a known malignancy (colorectal cancer, $n = 14$; lung cancer, $n = 5$; breast cancer, $n = 4$; non-Hodgkin's lymphoma, $n = 2$; ovarian cancer, $n = 1$; stomach carcinoma, $n = 1$; melanoma, $n = 1$, and an unknown primary, $n = 1$) and 1 patient with an indeterminate lung lesion. There were 9 men and 21 women (age range, 31–75 y; mean age ± SD, 59 ± 9.6 y). Indications for $^{18}$F-FDG were initial staging ($n = 9$), restaging of recurrence or metastatic spread ($n = 16$), monitoring response to treatment ($n = 2$), unexplained rising tumor markers ($n = 1$), characterization of a suspected lung lesion seen on CT ($n = 1$), and search for a primary tumor in a patient with a cervical metastatic lymph node ($n = 1$). All patients were monitored for at least 6 mo. The final diagnosis of scintigraphic lesions as representing active tumor sites was based on histology, correlation with other imaging modalities performed within 6 wk of the scintigraphic study, or imaging and clinical follow-up of at least 6 mo.

The patients fasted for at least 4 h before administration of $^{18}$F-FDG. Based on the patient's weight (200 μCi/kg), 370–700 MBq (10–19 mCi) $^{18}$F-FDG were injected intravenously. Each patient was imaged twice: once using a 5/8-in. crystal thickness dual-head γ-camera (CoDe5) and then with a 1-in. dual-head γ-camera (CoDe8). Acquisition started approximately 60 min after injection. The order in which the systems were used was randomized, depending on the availability of the cameras: Acquisition was started on the CoDe8 system followed by acquisition on the CoDe5 system in 18 patients and in the reverse order in the remaining12 patients. The information recorded for each patient included the body weight, injected dose, and waiting time between the injection and acquisition by each system. Each patient had a whole-body study consisting of 2 or 3 steps for imaging the chest, abdomen, and pelvis by the first system used. Then, 1 step ($n = 27$ patients) or 2 steps ($n = 3$) were repeated by the other system, thus yielding 33 coincidence studies available for comparison. The steps repeated were those relevant to the patient's disease—that is, imaging of the chest in the case of a lung cancer.

### Coincidence Techniques

Coincidence studies were performed using 2 dual-head γ-cameras modified to operate in the coincidence mode, with different detectors. The CoDe5 system with two 5/8-in. (16 mm) NaI(Tl) crystals (Millenium VG; General Electric Medical Systems) has been described in details in previous publications (*6,9*). The newly designed CoDe 8 system with two 1-in. (25.4 mm) NaI(Tl) crystals is equipped with an ultra-fast CoDe electronics (a CoDe VARICAM circuitry) and an integrated low-dose CT scanner (Discovery VH; General Electric Medical Systems). The increase in crystal thickness in the CoDe8 model results in a 60% increase in the crystal stopping-power efficiency (manufacturer's data). Dynamic segmentation of the detector field of view overcomes the challenge of the high counting rate. This segmentation permits the processing of the primary detected coincidence events without being affected by additional events hitting the detector during the processing period. Based on phantom studies performed according to NEMA 2001 (National Electrical Manufacturers Association), the specifications of the CoDe 8 system in coincidence mode are energy resolution of 11%, scatter fraction of 22%, axial reconstructed resolution of 5.5 mm, and transaxial reconstructed resolution of 6.5 mm (manufacturer's data).

In both systems, CoDe5 and CoDe8, random and scatter effects were minimized using a slit collimator that contains thin layers of lead, tin, and copper (graded absorber). This feature limits the axial acceptance angle and considerably reduces the probability of detecting noncoincidence events. In the CoDe8 system, the slit collimator acceptance angle was optimized according to the new front-end counting rate capability and to the scatter fraction effect on image quality. The high counting rate achieved by CoDe8 dictates setting the energy window in a high-resolution acquisition mode, collecting only photopeak events with 511 keV ± 10% (P–P mode). In the CoDe5, acquisition is done either in a high-resolution mode or in a "normal" or high-sensitivity acquisition mode in which, in addition to the peak events, Compton events caused by the partial-energy deposition of the 511-keV events in the detector crystal are also acquired. The energy window for these Compton events is 132–321 keV (P–C mode). The contribution of the scatter events within this energy window is minimized by the graded absorber. Data acquisition for each of the systems lasted 30 min per field of view, corresponding to 10 rotations of the gantry.

Integration of the CT detector in a coincidence γ-camera has been described in detail (*15,16*). The system consists of 384 crystals and photodiodes mounted on the gantry-rotating module. For transmission data, "half-scan" acquisition was performed over 220°, with each transaxial slice taking 16 s. Multiple slices were obtained by moving the table by a 1-slice step before acquiring the next slice. The full field of view consisting of 40 slices was completed in 10 min.

Transmission data of the patient were corrected and reconstructed using a filtered backprojection to produce cross-sectional attenuation images in which each pixel represents the attenuation of the imaged tissue. The transmission data were used to correct the emission data for the effect of photon attenuation as well as for generating the coincidence-CT (functional–anatomic) fused images.

An iterative reconstruction algorithm, coincidence list ordered-set expectation maximization, which is a 3-dimensional algorithm, was used (*9*). Reconstruction as well as fusion of coincidence and CT images was performed on the eNTEGRA workstation (Elgems) (*6,9*).

### Analysis of Results

*Accepted Coincidence Events.* The number of accepted events in CoDe5 acquisition and in CoDe 8 acquisition was compared. This number was corrected for decay according to the waiting time between the injection and acquisition.

*Tumor Detection and Image Quality Parameters.* Each patient had 4 different image sets for comparison: CoDe5 images without attenuation correction (CoDe5NC), CoDe8 images without attenuation correction (CoDe8NC), CoDe8 images with attenuation correction (CoDe8AC), and fused images of CoDe8AC and low-resolution CT (fused images).

The visual assessment was aimed to compare tumor detection rate on the various image sets. In addition, it assessed the added clinical value of fusion of the coincidence data with CT. For the purpose of this study, CoDe5 and CoDe8 images were interpreted in sequential steps on separate days, at least 1 wk apart; the patient's name was removed from the report; and the images were presented in a different patient's order for the repeated interpretation. The final diagnosis of scintigraphic lesions as tumor sites was drawn on histology, correlation with other imaging modalities, or clinical follow-up of at least 6 mo.

For quantitative assessment, the activity in tumor sites, physiologic uptake, and background activity were measured as follows:

- Target activity (tumor): The operator identified the lesion. The first slice and the last slice in which this lesion was detected were selected. A region of interest (ROI) surrounding the lesion was drawn in the slice in which the lesion was best seen, and this ROI was copied onto all ensuing slices. Pixels in all slices containing the lesion were added together, and the sum was multiplied by the slice thickness, thus creating the functional volume of the tumor. The target activity was defined as the average activity value (counts) in the functional volume.
- Nontarget activity: Physiologic bone uptake at the sternum or the sacrum was used as the site of nontarget uptake. The selection of bone as the nontarget organ was based on the fact that findings in other physiologic sites of $^{18}$F-FDG uptake, such as the bowel or the urinary system, may be altered when moving the patient from one system to the other.
- Background activity: The background was selected adjacent to the tumor.

On the basis of these measurements, 2 image quality parameters were generated: a target-to-nontarget ratio (T/NT ratio) and a target-to-background ratio (T/Bg ratio). These parameters were determined for active tumor sites on 3 image sets—that is, the CoDe5NC, CoDe8NC, and CoDe8AC images. The impact of the detector design on image quality was assessed by comparing the T/TN and T/Bg values obtained on the nonattenuated images of the CoDe5 and CoDe8 systems (CoDe5NC vs. CoDe8NC). The impact of attenuation correction on image quality was assessed by comparing the T/NT and T/Bg values obtained on the attenuated and nonattenuated CoDe8 images.

For each of the systems, the T/NT ratios measured for lesions were separated into 2 groups based on the waiting time after injection. Two hours was the time point separating "early" from "late" studies. The purpose of this evaluation was to exclude the difference in waiting time from injection to acquisition between the 2 systems as a potential source of the difference in the activity measurements and in the lesion detectability.

### Statistical Analysis

A paired *t* test and 95% confidence intervals (95% CIs) were used for comparing the T/Bg and T/NT ratios between the CoDe5 and CoDe8 systems and between the CoDe8 images with and without attenuation correction. A *t* test was used to compare the number of accepted events by the systems in each of the patients. A $P$ value $< 0.05$ was considered statistically significant.

## RESULTS

### Accepted Coincidence Events

The number of accepted events obtained in the high-resolution mode (counting the events with an energy window setting of 511 keV ± 10%) by the CoDe8 was significantly higher than the number of accepted events obtained by CoDe5 (5.21 ± 1.46 million vs. 1.27 ± 0.36 million, $P < 0.001$). The number of accepted events obtained by the CoDe5 in a high-sensitivity mode (counting the peak events with 511 keV ± 10% as well as Compton events of 132–321 keV) was 3.82 ± 1.08 million.

### Tumor Detection

Six of the study patients had a negative $^{18}$F-FDG study. In the remaining 24 patients, $^{18}$F-FDG assessment revealed 61 active tumor sites. The final diagnosis of the scintigraphic lesions as representing active tumor tissue was based on histopathology ($n = 11$ patients); on correlative findings on other imaging modalities, including colonoscopy, CT, MRI, and transrectal ultrasonography ($n = 7$ patients); and on imaging and clinical follow-up of at least 6 mo ($n = 6$ patients).

*Visual Assessment.* Of the 61 tumor sites detected on the CoDe8AC images, 59 (97%) were detected on the

CoDe8NC images and 54 lesions (88%) were detected on the CoDe5 images. The lesions missed by the CoDe5NC images included 3 liver metastases and 4 metastatic lymph nodes, 3 located in the abdomen and 1 in the mediastinum (Fig. 1). The 54 tumor sites detected by all 3 image sets were used in the quantitative analysis. The 7 lesions missed by CoDe 5 occurred in 5 patients (in 2 patients, CoDe5 was used first).

Fused coincidence-CT images improved image interpretation in 10 of 30 patients (33%), and this was of clinical relevance in 6 of 30 patients (20%) (Table 1; Fig. 2).

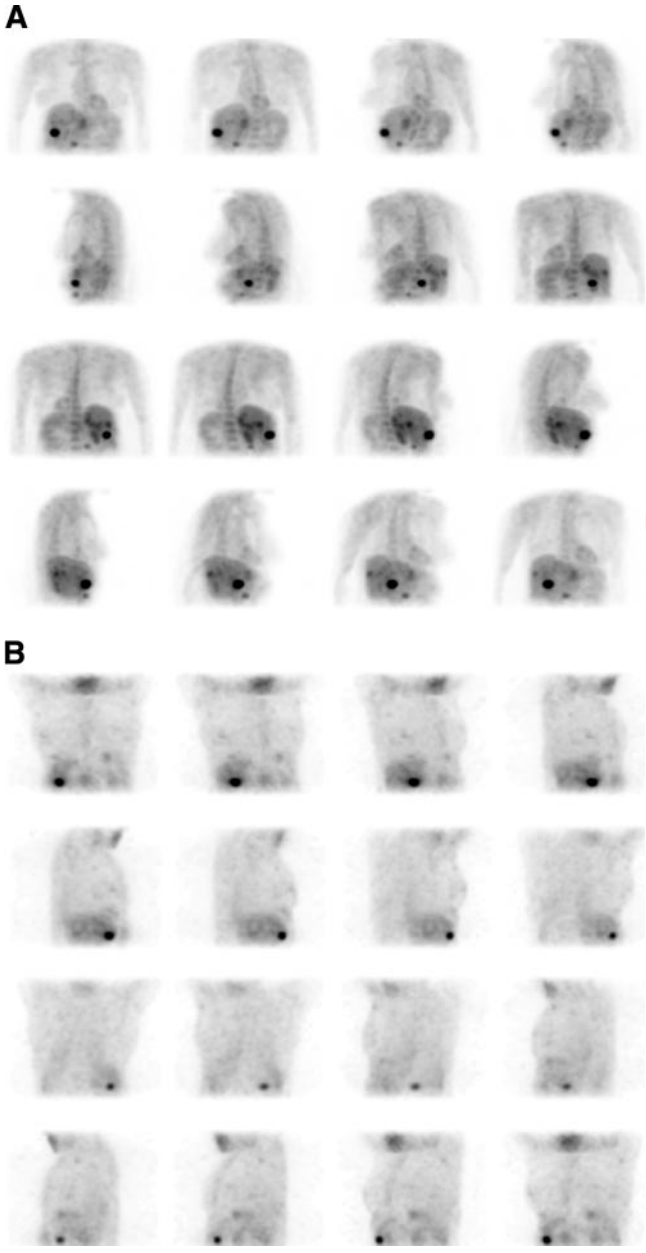


**FIGURE 1.** A 64-y-old patient with known colorectal cancer. $^{18}$F-FDG study was performed for restaging before surgical removal of solitary liver metastasis originally observed on CT. (A) 3-Dimensional maximum-intensity-projection (MIP) images of CoDe5 without attenuation correction detected single lesion in liver. (B) 3-Dimensional MIP images of CoDe8 with attenuation correction detected multiple liver lesions in both liver lobes. Patient's management was altered by planned surgery being canceled and patient being referred for chemotherapy and radiofrequency treatment.

*Quantitative Assessment.* This analysis was performed on the 54 tumor sites detected by all 3 image sets: CoDe5NC, CoDe8NC, and CoDe8AC. Tumor sites were categorized based on their location (above and below the diaphragm). Diagnostic CT was available for correlation, and lesion size was determined in all but 9 scintigraphically detected tumor sites. However, these measurements do not accurately determine the tumor size at the time of scintigraphy because of the time gap between the procedures. Instead, the tumor size was estimated by the functional volumes. Descriptive statistics were performed to define the limits of the 4 subgroups: lesions <7.2 mL (mean CT size, 1.2 cm), 7.2–12.5 mL (mean CT size, 1.7 cm), 12.5–17.5 mL (mean CT size, 1.95 cm), and lesions <17.5 mL (mean CT size, 3.1 cm):

- Comparison of image quality between systems with different detectors: CoDe5NC versus CoDe8NC images—The mean T/NT ratio and T/Bg ratio values in all 54 tumor sites analyzed were significantly higher on the CoDe8 images. The superiority of the thicker crystal was more pronounced in lesions located above the diaphragm as well as in small-volume lesions. In large lesions, no significant difference was found between the 2 systems (Table 2).
- Comparison of image quality between attenuated and nonattenuated images: CoDe8NC versus CoDe8AC—The mean T//Bg ratio was significantly higher on the attenuated images for lesions located above and below the diaphragm as well as for lesions of all functional volumes (Table 3).
- Influence of waiting time: In the CoDe5 images, the mean T/NT ratio was 3.7 ± 2.4 for lesions detected on early CoDe5 studies and 3.3 ± 2.4 ($P$ = not significant [NS]) for lesions detected on late CoDe5 studies. A similar comparison was 3.96 ± 1.7 versus 5.2 ± 3.9 ($P$ = NS) for early and late CoDe8NC images and 4.1 ± 1.3 versus 6.5 ± 3.4 ($P$ = NS) for early and late CoDe8AC images.

## DISCUSSION

The purpose of this study was to compare the performance of 2 coincidence γ-camera systems differing in their NaI(Tl) crystal design: the CoDe5 system equipped with 5/8-in. detectors and the CoDe8 system equipped with 1-in. detectors. The CoDe8 is also equipped with an integrated x-ray transmission system for attenuation correction and image fusion. The study was clinical, assessing both tumor detection and image quality. According to the study design, comparison was direct in patients who underwent an $^{18}$F-FDG study using both cameras during the same visit.

Scintigraphic detection of lesions is proportional to the size and the contrast of the lesions and is inversely proportional to the reconstructed resolution and the statistical noise in the image (*17*). The lower the number of counts in the image, the higher the statistical noise. Therefore, improved

**TABLE 1**
Added Value of Fusion of Coincidence and CT to Image Interpretation and Patient Management

| Tumor type | Coincidence results alone | Fused image results | Added value of fused images to image interpretation | Added value of fused images to patient management |
|---|---|---|---|---|
| Lung cancer | Parahilar uptake | Localization of uptake to lung parenchyma, no evidence of LN involvement | Better anatomic localization, exclusion of nodal involvement | Accurate staging, referral for surgery |
| Lung cancer | Uptake in lung tumor and in additional abdominal site | Localization of abdominal site of uptake at left adrenal | Better anatomic localization, detection of metastatic spread | Accurate staging, referral for chemotherapy |
| Colorectal cancer | Uptake in right anterior abdomen | Uptake localized in ectopic kidney | Differentiation of physiologic from tumor uptake | Exclusion of disease |
| Colorectal cancer | Perirectal uptake | Focus of uptake in large perirectal residual mass | Better anatomic localization, detection of viable tissue within fibrosis | None |
| Colorectal cancer | Uptake in right upper abdomen | Physiologic uptake in hepatic flexure of colon | Differentiation of physiologic from tumor uptake | None |
| Colorectal cancer | Presacral and perineal uptake | Uptake in pelvic masses and in adjustment LNs | Better anatomic localization, detection of nodal involvement | None |
| Colorectal cancer | Pelvic uptake | Pelvic uptake extending to sacrum | Better anatomic localization, detection of adjacent bone involvement | Referral for radiotherapy to involved bone |
| Breast cancer | Uptake in left pelvis | Localization of uptake to iliac crest | Better anatomic localization, detection of bone involvement | None |
| Breast cancer | Uptake in breast and in paratracheal region | Localization of cervical uptake in thyroid nodule | Better anatomic localization, detection of unsuspected thyroid lesion | Thyroid lesion was found to be second primary tumor; breast and thyroid tumors were removed |
| Unknown primary | Sites of uptake in cervical, oropharynx, and retrosternal regions | Oropharynx uptake delineated lesion at that location on CT image; retrosternal uptake was located in postsurgical changes | Better anatomic localization, detection of unknown primary tumor, exclusion of disease in region of previous surgery | Referral for surgery and radiotherapy |

LN = lymph node.

system sensitivity may reduce image noise. In the current study, the number of accepted coincidence events was significantly higher on the CoDe8 system. Because the acquisition time on both systems was similar and the patient's parameters were identical, the higher number of accepted events probably reflects an improved system sensitivity of the CoDe 8 system when assessed clinically.

An increase in NaI(Tl) crystal thickness was found to improve system sensitivity for coincidence imaging in a previous study (*18*) that compared the performance of a CoDe5 system with that of a coincidence system equipped with 3/8-in. crystals (CoDe3), a crystal thickness used in the routine practice of nuclear medicine. On a phantom study, lesion detectability was similar for both CoDe5 and CoDe3 systems. However, the camera equipped with the thicker crystals was characterized by an improved volume sensitivity. On a clinical assessment, the CoDe5 system detected only a small number of additional lesions compared with those detected by the CoDe3 system: 78% versus 73% of lesions (*18*). Similarly, in the current study, 54 of the 59 tumor sites detected on the CoDe8 images without attenuation correction were detected also on the CoDe5 images. A more significant difference was found with regard to image quality, which was improved on the images obtained by the system with the thicker detectors. Higher T/NT and T/Bg ratios were obtained on the CoDe8 images, particularly in smaller lesions and in lesions detected above the diaphragm.

The impact of attenuation correction in coincidence imaging was assessed in this study for the CoDe8 camera. Only 2 additional tumor sites were detected on the attenuation-corrected images compared with the noncorrected images. These results resemble the previous experience at Vanderbilt University Medical Center with the CoDe5 camera (*1,9*). In the latter studies, CoDe5AC images detected 78% and CoDe5NC images detected 75% of the lesions that were detected on the images obtained by a dedicated PET system. Chan et al. reported a better tumor staging on the corrected images (*19*). Although it may not always improve the overall lesion detection rate, attenuation-corrected images have been previously reported to improve image quality as well as to provide a better anatomic delineation of lesions (*8–11,19*). In the current study, the T/Bg ratios obtained on the corrected images were higher for a large range of lesion sizes and tumor locations.

For some years, a debate developed around image coregistration. Image coregistration of data arising from different technologies was labor intensive. The new generation of hybrid systems composed of a dedicated PET system and a diagnostic CT system is now regarded as a new imaging tool with improved diagnostic accuracy (*20*). Although the

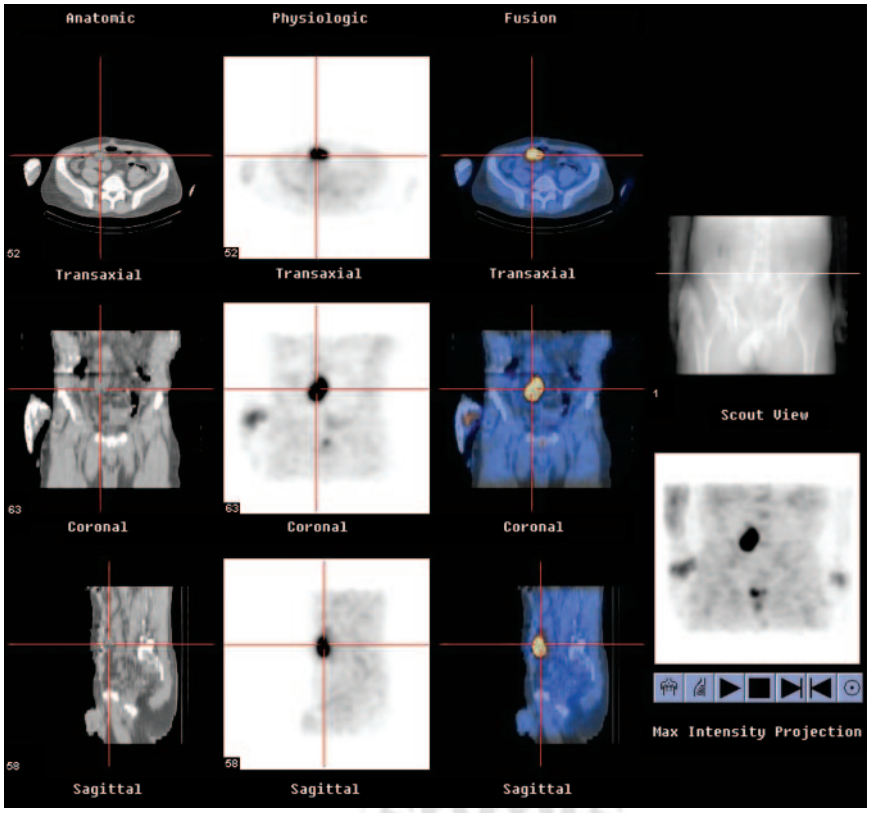


**FIGURE 2.** A 57-y-old patient with known colorectal cancer was referred for $^{18}$F-FDG study because of rising carcinoembryonic antigen levels. Coincidence images detected increased uptake in anterior abdomen. Fusion of coincidence data with low-resolution CT image localized uptake in dilated collecting system of right ectopic kidney. Patient was disease free on clinical follow-up.

CT installed in the coincidence γ-camera is of low resolution and does not replace the diagnostic CT, emerging data support the impression that fusion of the SPECT or coincidence data with low-resolution CT improves diagnostic accuracy (*1,9,21*). The impact of fusing the coincidence data with the low-resolution CT data was determined in the current study by comparing the interpretation of CoDe8AC images alone with fused images of CoDe8AC with CT: Fused images improved image interpretation in one third of the patients. In 6 of 30 study patients (20%), the data added by the fusion were clinically relevant to patient management.

There are several limitations to the current study. Not all patients had contemporaneous diagnostic CT or histology of all detected lesions and, therefore, it was not possible to assess the overall diagnostic accuracy of coincidence imaging in this study. However, because the purpose of the study was to compare 2 imaging systems, images obtained by the system with the thicker detector and attenuation correction were the reference for comparison. We could not determine the actual size for all tumor sites detected on the coincidence images. Correlation between imaging modalities performed within 6 wk of each other is acceptable if it aims to determine the final diagnosis of the lesions and has been used in the current study as a standard of reference. CT-measured tumor size, however, was not an accurate reference for the scintigraphic lesion size because of the time gap between the 2 studies. The low-resolution CT data of the CoDe8 system was not appropriate for size measurements, particularly in the case of smaller lesions. Because a critical mass is always necessary for a lesion to be visualized on scintigraphy, we used the functional volume as a parameter to estimate the tumor size. The functional volume of an $^{18}$F-FDG–avid disease has been found in PET studies to be a clinically relevant parameter with a prognostic impact (*22*).

Another limitation is the different waiting times from injection to acquisition with each of the systems. Because the principal design of the study was to perform both studies during the same visit, this difference was inevitable. To minimize its impact on the study results, the order of systems was randomized. Randomization was not optimal, as more patients were scanned with the 1-in. system first. When assessing the impact of the waiting time, for each of the systems, T/NT ratios measured in lesions detected on early studies were not statistically different from the ratios measured in lesions detected on delayed images. Lesions seen on CoDe8 and missed on CoDe5 images occurred also in patients in whom the latter was used first.

The manufacturer's software permitted scanning with the 5/8-in. system in both the P–P and the P–C modes but only with the P–P mode in the case of the 1-in. system. This fact in the study design may have introduced some bias in the results.

## CONCLUSION

The results of this study suggest that the increase of the NaI(Tl) crystal thickness and attenuation correction improve image quality and, to a lesser extent, the tumor detection rate in coincidence imaging. Fused coinci-

**TABLE 2**
Impact of NaI(Tl) Detector Thickness on Image Quality

| Parameter | CoDe5NC | CoDe8NC | *P** | 95% CI |
|---|---|---|---|---|
| All tumor lesions ($n$ = 54) | | | | |
| T/NT ratio | 4.2 ± 3.5 | 6.3 ± 5.2 | <0.0005 | 1.3, 3.0 |
| T/Bg ratio | 4.9 ± 3.9 | 6.4 ± 5 | <0.0005 | 0.8, 2.3 |
| Assessment of lesions according to location | | | | |
| Above diaphragm ($n$ = 31) | | | | |
| T/NT ratio | 4.5 ± 4 | 7.1 ± 5.7 | <0.0005 | 1.3, 3.9 |
| T/Bg ratio | 5.25 ± 4.6 | 7.5 ± 5.7 | <0.0005 | 1.1, 3.4 |
| Below diaphragm ($n$ = 23) | | | | |
| T/NT ratio | 3.7 ± 2.6 | 5.2 ± 4.3 | <0.001 | 0.6, 2.4 |
| T/Bg ratio | 4.3 ± 2.7 | 4.8 ± 3.3 | NS | −0.3, 1.4 |
| Assessment of lesion of different sizes† | | | | |
| Lesions <7.2 mL ($n$ = 14) | | | | |
| T/NT ratio | 3.6 ± 2.8 | 6.2 ± 4.7 | <0.001 | 1.2, 4.0 |
| T/Bg ratio | 4 ± 3 | 6.6 ± 4.3 | <0.0005 | 1.4, 3.6 |
| Lesions 7.2–12.5 mL ($n$ = 13) | | | | |
| T/NT ratio | 4.2 ± 3.7 | 6 ± 2.7 | <0.01 | 0.3, 3.4 |
| T/Bg ratio | 4.6 ± 3 | 6.5 ± 3.3 | <0.03 | −0.02, 3.9 |
| Lesions 12.5–17.5 mL ($n$ = 14) | | | | |
| T/NT ratio | 4.4 ± 4 | 7 ± 7.7 | <0.01 | 0.4, 4.9 |
| T/Bg ratio | 5 ± 3.8 | 6.4 ± 6.4 | <0.05 | −0.3, 3.2 |
| Lesions >17.5 mL ($n$ = 13) | | | | |
| T/NT ratio | 4.5 ± 3.5 | 6 ± 4.9 | NS | −0.5, 3.3 |
| T/Bg ratio | 6 ± 5.4 | 6 ± 5.7 | NS | −1.3, 1.5 |

*$P < 0.05$ was considered significant. NS = not significant.

†Parameters evaluated: T/NT ratio and T/Bg ratio. Lesion size was measured by functional volumes. Descriptive statistics were used to define 4 subgroup limits.

Image sets compared were CoDe5NC, 5/8-in. NaI(Tl) crystals without attention correction; and CoDe8NC, 1-in. NaI(Tl) crystals without attention correction.

**TABLE 3**
Impact of Attenuation Correction on Image Quality

| Parameter | CoDe8NC | CoDe8AC | *P** | 95% CI |
|---|---|---|---|---|
| All tumor lesions ($n$ = 54) | | | | |
| T/NT ratio | 6.3 ± 5.2 | 7.5 ± 5.8 | <0.05 | −0.2, 2.8 |
| T/Bg ratio | 6.4 ± 5 | 8.9 ± 5.6 | <0.0005 | 1.4, 3.8 |
| Assessment of lesions according to location | | | | |
| Above diaphragm ($n$ = 31) | | | | |
| T/NT ratio | 7.1 ± 5.7 | 9.0 ± 6.4 | <0.04 | −0.1, 4.1 |
| T/Bg ratio | 7.5 ± 5.7 | 10.4 ± 6.2 | <0.001 | 1.2, 4.6 |
| Below diaphragm ($n$ = 23) | | | | |
| T/NT ratio | 5.2 ± 4.3 | 5.6 ± 4.2 | NS | −1.8, 2.5 |
| T/Bg ratio | 4.8 ± 3.3 | 7 ± 4.1 | <0.003 | 0.4, 3.9 |
| Assessment of lesion $n$ of different sizes† | | | | |
| Lesions <7.2 mL ($n$ = 14) | | | | |
| T/NT ratio | 6.2 ± 4.7 | 8.7 ± 5.3 | NS | −0.2, 5.6 |
| T/Bg ratio | 6.6 ± 4.3 | 9.9 ± 4.4 | <0.01 | 1.2, 5.7 |
| Lesions 7.2–12.5 mL ($n$ = 13) | | | | |
| T/NT ratio | 6 ± 2.7 | 8.3 ± 7.6 | NS | −2.0, 6.5 |
| T/Bg ratio | 6.5 ± 3.3 | 10.1 ± 6.9 | <0.03 | −0.1, 7.3 |
| Lesions 12.5–17.5 mL ($n$ = 14) | | | | |
| T/NT ratio | 7 ± 7.7 | 7.4 ± 6.3 | NS | −2.6, 3.3 |
| T/Bg ratio | 6.4 ± 6.4 | 7.94 ± 4.6 | <0.03 | −0.8, 3.9 |
| Lesions >17.5 mL ($n$ = 13) | | | | |
| T/NT ratio | 6 ± 4.9 | 5.7 ± 3.5 | NS | −3.1, 2.5 |
| T/Bg ratio | 6 ± 5.7 | 7.8 ± 6.6 | <0.03 | −0.04, 3.7 |

*$P < 0.05$ was considered significant. NS = not significant.

†Parameters evaluated: T/NT ratio and T/Bg ratio. Lesion size was measured by functional volumes. Descriptive statistics were used to define 4 subgroup limits.

Image sets compared were 1-in. NaI(Tl) crystals with and without attenuation correction (CoDe8NC and CoDe8AC).

dence-CT images add data that are clinically relevant in 20% of the patients.

## REFERENCES


1. Delbeke D, Sandler MP. The role of hybrid cameras in oncology. *Semin Nucl Med.* 2000;30:268–280.
2. Kunze WD, Baehre M, Richter E. PET with a dual-head coincidence camera: spatial resolution, scatter fraction, and sensitivity. *J Nucl Med.* 2000;41:1067–1074.
3. Inoue T, Oriuchi N, Koyama K, et al. Usefulness of dual-head coincidence gamma camera with thick NaI crystals for nuclear oncology: comparison with dedicated PET camera and conventional gamma camera with thin NaI crystals. *Ann Nucl Med.* 2001;15:141–148.
4. Ak I, Blokland JAK, Pauwels EKL, Stokkel MPM. The clinical value of $^{18}$F-FDG detection with a dual-head coincidence camera: a review. *Eur J Nucl Med.* 2001;28:763–778.
5. Gambhir SS, Czernin J, Schwimmer J, Silverman DH, Coleman RE, Phelps ME. A tabulated summary of the FDG PET literature. *J Nucl Med.* 2001; 42(suppl):1S–93S.
6. Even-Sapir E, Lerman H, Figer A, et al. Role of $^{18}$F-FDG dual-head gamma-camera coincidence imaging in recurrent or metastatic colorectal carcinoma. *J Nucl Med.* 2002;43:603–609.
7. Wahl RL. To AC or not to AC: that is the question. *J Nucl Med.* 1999;40: 2025–2028.
8. Coleman RE, Laymon CM, Turkington TG. FDG imaging of lung nodules: a phantom study comparing SPECT, camera-based PET, and dedicated PET. *Radiology.* 1999;210:823–828.
9. Delbeke D, Martin WH, Patton JA, Sandler MP. Value of iterative reconstruction, attenuation correction and image fusion in the interpretation of FDG PET images with an integrated dual-head coincidence camera and x-ray-based attenuation maps. *Radiology.* 2001;218:163–171.
10. Zimny M, Kaiser HJ, Cremerius U, et al. Dual-head gamma camera 2-[fluorine-18]-fluoro-2-deoxy-D-glucose positron emission tomography in oncological patients: effects of non-uniform attenuation correction on lesion detection. *Eur J Nucl Med.* 1999;26:818–823.
11. Paul AK, Tatsumi M, Yutani K, Fujino K, Hashikawa K, Nishimura T. Effects of iterative reconstruction on image contrast and lesion detection in gamma camera coincidence imaging in lung and breast cancers. *Nucl Med Commun.* 2002;23:103–110.
12. Zhang H, Inohu T, Tian M, et al. A basic study on the lesion detectability for hot spot imaging of positron emitters with dedicated PET and positron coincidence gamma camera. *Ann Nucl Med.* 2001;15:301–306.
13. Shreve PD, Steventon RS, Deters EC, Kison PV, Gross MD, Wahl RL. Oncologic diagnosis with 2-[fluorine-18]fluoro-2-deoxy-D-glucose imaging: dual-head coincidence gamma camera versus positron emission tomographic scanner. *Radiology.* 1998;207:431–437.
14. Zhang H, Tian M, Oriuchi N, Tanada S, Endo K. Oncological diagnosis using positron coincidence gamma camera with fluorodeoxyglucose in comparison with dedicated PET. *Br J Radiol.* 2002;75:409–416.
15. Patton JA, Delbeke D, Sandler MP. Image fusion using an integrated, dual-head coincidence camera with x-ray tube-based attenuation maps. *J Nucl Med.* 2000;41:1364–1368.
16. Bocher M, Balan A, Krausz Y, et al. Gamma camera-mounted anatomical x-ray tomography: technology, system characteristics and first images. *Eur J Nucl Med.* 2000;27:619–627.
17. Mullani NA. Comparing diagnostic accuracy of gamma camera coincidence systems and PET for detection of lung lesions. *J Nucl Med.* 2000;41:959–960.
18. Boren EL Jr, Delbeke D, Patton JA, Sandler MP. Comparison of FDG PET and positron coincidence detection imaging using a dual-head camera with 5/8-inch NaI (Tl) crystals in patients with suspected body malignancies. *Eur J Nucl Med.* 1999;26:379–387.
19. Chan WL, Freund J, Pocock NA, et al. Coincidence detection FDG PET in the management of oncological patients: attenuation correction versus non-attenuation correction. *Nucl Med Commun.* 2001;22:1185–1192.
20. Ell PJ, von Schulthess GK. PET/CT: a new road map. *Eur J Nucl Med.* 2002;29:719–720.
21. Even-Sapir E, Keidar Z, Sachs J, et al. The new technology of combined transmission and emission tomography (TET) in the evaluation of endocrine neoplasms. *J Nucl Med.* 2001;42:998–1004.
22. Wang W, Larson SM, Fazzari M, et al. Prognostic value of [F18]fluorodeoxyglucose positron enission tomography scanning in patients with thyroid cancer. *Clin Endocrinol Metab.* 2000;85:1107–1113.